

Effect of hydrostatic pressure upon the magnetic transitions in the $\text{Gd}_5(\text{Si}_x\text{Ge}_{1-x})_4$ giant magnetocaloric compounds: X-ray magnetic circular dichroism study

Y. C. Tseng,^{1,2} D. Haskel,^{2,*} J. C. Lang,² S. Sinogeikin,³ Ya. Mudryk,⁴ V. K. Pecharsky,⁴ and K. A. Gschneidner, Jr.⁴

¹Department of Materials Science and Engineering, Northwestern University, Evanston, Illinois 60201, USA

²Magnetic Materials Group, Advanced Photon Source, Argonne National Laboratory, Argonne, Illinois 60439, USA

³HPCAT, Carnegie Institution of Washington, Advanced Photon Source, Argonne National Laboratory, Argonne, Illinois 60439, USA

⁴Materials and Engineering Physics Program, Ames Laboratory, Iowa State University, Iowa 50011, USA

(Received 27 April 2007; published 10 July 2007)

The pressure dependence of the magnetic transitions in the giant magnetocaloric materials $\text{Gd}_5(\text{Si}_x\text{Ge}_{1-x})_4$ ($x=0.125, 0.5$) has been investigated using x-ray magnetic circular dichroism (XMCD) measurements in a diamond anvil cell (DAC). We found that the most notable features of the x - T phase diagram are also present in the P - T phase diagram. These include a nearly linear increase in Curie temperature, T_c , with increasing both x and P up to 275 K, and a discontinuity accompanied by a change in slope, $dT_c/d(x, P)$, at this temperature. However, the results indicate that a similar volume change results in ~ 3 times larger increase in T_c with Si doping than with pressure. Si doping, hence, does more to stabilize ferromagnetic interactions than simply uniformly reducing the unit cell volume.

DOI: [10.1103/PhysRevB.76.014411](https://doi.org/10.1103/PhysRevB.76.014411)

PACS number(s): 75.70.-i, 75.75.+a, 75.25.+z

I. INTRODUCTION

Magnetocaloric materials have recently attracted much attention due to their potential for use in magnetic refrigeration.¹⁻⁷ Among these materials, $\text{Gd}_5(\text{Si}_x\text{Ge}_{1-x})_4$ compounds are promising because they display a field-induced, tunable first-order magnetostructural transition,^{4,6} making them attractive candidates for magnetic refrigeration near room temperature. The magnetism and crystallography exhibited by these compounds depend on Si content (x) and can be categorized into three regions. In the compositional range $0.24 \leq x \leq 0.5$, the giant magnetocaloric effect (MCE)⁶ is related to a first-order, magnetic-crystallographic phase transition, in which a paramagnetic (PM) to ferromagnetic (FM) transition on cooling is accompanied by a change in crystal structure from a monoclinic (M) to an orthorhombic [$O(\text{I})$] phase.⁷⁻⁹ The most notable feature of this phase transition is the reversible breaking and reforming of covalent Ge(Si)-Ge(Si) bonds connecting Gd-containing slabs, which occurs concomitantly with the change of magnetic state. The crystal structure changes via a martensiticlike mechanism, involving large shear displacements ($\approx 0.5 \text{ \AA}$) of subnanometer-thick Gd-containing slabs.^{7,9} Since this reversible phase transition can be manipulated by application of a magnetic field, most investigations⁷⁻¹¹ of these materials have been carried out within this compositional range. In particular, $\text{Gd}_5\text{Si}_2\text{Ge}_2$ is the most studied, because it has a large magnetic entropy change due to a first-order magnetostructural transition occurring near ambient temperature.⁷⁻¹¹

In the Si-rich region $0.5 \leq x \leq 1.0$, the material undergoes a second-order PM to FM transition on cooling without an accompanying structural change: the structure remains $O(\text{I})$ in both PM and FM phases, and all slab-connecting bonds remain present. The Ge-rich alloys ($0 \leq x \leq 0.2$), on the other hand, exhibit two phase transitions on cooling: a second-order PM to antiferromagnetic (AFM) transition and a first-order AFM to FM transition at lower temperatures. This second transition is accompanied by a structural transition between two orthorhombic polymorphs, i.e., between the so-called $O(\text{II})$ -type structure and $O(\text{I})$.¹²

Since Si and Ge atoms have markedly different sizes, the unit cell volume is affected by the Si/Ge ratio. Silicon doping contracts the lattice, promoting slab-connectivity and ferromagnetic ordering. Similarly, hydrostatic pressure has been used to affect magnetic and structural properties.¹³⁻¹⁶ Morellon *et al.*¹³ reported that these magnetocaloric compounds exhibit a pressure-induced increase of the magnetic transition temperature $dT_c/dP=0.3 \text{ K kbar}^{-1}$ for a Si-rich sample with $x=0.8$. The increase is more significant in the $0 \leq x \leq 0.5$ range, for which $dT_c/dP=3.0 \text{ K kbar}^{-1}$ ($x=0.1, 0.45$) has been reported, indicating that ferromagnetic ordering is most greatly stabilized by a volume contraction in this region. Unquestionably, hydrostatic pressure is able to alter the magnetic transition. Experimental investigations of the equivalency of chemical doping and pressure, however, have been limited to relatively low applied pressures. Most pressure-related research in $\text{Gd}_5(\text{Si}_x\text{Ge}_{1-x})_4$ compounds was done using the strain-gauge technique in a piston-cylinder, which can only provide pressures up to $\approx 1 \text{ GPa}$ (10 kbar). The highest pressure applied to $\text{Gd}_5(\text{Si}_x\text{Ge}_{1-x})_4$ was 25 kbar, as reported in the pressure-induced polymorphism study of Mudryk *et al.*¹⁴

The goal of this work is to extend the pressure range of these studies up to $\approx 150 \text{ kbar}$ in order to better explore the correlation between Si content and applied pressure (P) upon the magnetic transitions over this extended pressure range. In addition to causing a volume contraction, substitution of Ge by Si may introduce changes in the electronic band structure; hence, pressure studies provide a better way to isolate the effects of volume reduction upon the magnetic properties. To this end, we have adapted a diamond anvil cell (DAC) to permit x-ray magnetic circular dichroism (XMCD)¹⁷ measurements in order to obtain element-specific magnetization data on these compounds at hydrostatic pressures up to 15 GPa (150 kbar). Furthermore, this same setup permits energy scanning over an extended energy range, therefore the x-ray absorption fine structure (XAFS)¹⁸ spectra can be obtained on a standard material to perform *in situ* pressure calibration. Below we present the experimental details and re-

sults of these experiments, followed by a detailed discussion.

II. EXPERIMENT

Polycrystalline samples of $\text{Gd}_5(\text{Si}_x\text{Ge}_{1-x})_4$ were prepared as described by Pecharsky and Gschneidner.⁷ In addition, the alloys were heat treated at 1300 °C for 1 h. Fine powders ($\leq 1 \mu\text{m}$) of these samples were thoroughly mixed with equally fine powders of Cu and dispersed in silicon oil which was used as hydrostatic pressure medium. The Cu powder serves as an *in situ* pressure calibrant for these measurements, as discussed below. The volume ratios, optimized for absorption measurements at Gd L_3 and Cu K edges, were 1:1:17 for $\text{Gd}_5(\text{Si}_x\text{Ge}_{1-x})_4$, Cu, and silicon oil, respectively. The mixture was loaded into a 250 μm hole in a nonmagnetic stainless steel gasket, which was preindented to a thickness of 80 μm . The copper-beryllium DAC is suitable for low-temperature measurements and is manufactured by EasyLab Technologies (previously Diacell).

The diamond anvils were perforated to minimize x-ray absorption and allow high-quality transmission x-ray data to be collected over the Gd L_3 (7.243 keV) and Cu K (8.979 keV) edges. The diamond configuration is similar to that described by Dadashev *et al.*¹⁹ It consists of a fully perforated diamond anvil, which serves as a backing plate for a mini-anvil 0.7 mm high, and an opposing, partially perforated anvil (PPA) with a 0.2 mm inner wall. The minianvil and PPA have 0.45 mm culets, allowing pressures of ≈ 15 GPa to be reached. The DAC was mounted on the cold finger of a He-flow cryostat, itself mounted on high-resolution translation stages. The cryostat was placed between the pole pieces of an electromagnet, which provided a maximum magnetic field strength of 0.7 Tesla. The pressure could be varied *in situ* during low-temperature measurements without having to remove the cell from the cryostat, by controlling piston motion via the He gas pressure in an expanding membrane.

The x-ray measurements were carried out at beamline 4-ID-D of the Advanced Photon Source at Argonne National Laboratory.²⁰ A toroidal Pd focusing mirror was used to focus the central $1 \times 1 \text{ mm}^2$ portion of the undulator beam to a $\sim 170 \times 200 \mu\text{m}^2$ spot size. The beam was further reduced to $50 \times 50 \mu\text{m}^2$ by a limiting aperture placed just before the cell (this final beam size was smaller than the aperture in the perforated anvils). Circularly polarized x rays were generated by phase-retarding optics,^{21,22} and the XMCD measured by modulating the x-ray helicity at 12.7 Hz and detecting the related modulation in the absorption coefficient with a lock-in amplifier.²³

Copper K -edge XAFS was used to calibrate the pressure in the sample chamber at each pressure point. The pressure-induced volume change in Cu was determined by fitting the XAFS data using FEFF6.0 theoretical standards²⁴ and the IFEFFIT 2.8 package.²⁵ Pressure was determined by comparing to the known Cu compressibility curve.²⁶ The XMCD measurements at the Gd L_3 edge were carried out on warming after zero-field cooling to 20 K, and Cu K -edge XAFS was measured at 300 K.

III. RESULTS

The pressure dependence of the magnetic transition was measured in the 0.25–14.55 GPa range. Figure 1 shows temperature-dependent Gd L_3 -edge XMCD data for the $x=0.125$ sample at applied pressures of 0.25 GPa [Fig. 1(a)] and 14.55 GPa [Fig. 1(b)]. The inset figures show that the XMCD signal fully reverses upon reversal of a 0.7 Tesla applied field, as expected. The XMCD signal at $P=0.25$ GPa does not change significantly from 20 to 80 K, but drops quickly at ~ 90 K. This drop is due to the magnetostructural, first-order phase transition, which at ambient pressure occurs at 80 K (Refs. 4, 6, and 16) as confirmed with XMCD measurements outside the DAC.²⁷ At $P=14.55$ GPa the magnetic transition has significantly shifted upward in temperature.

Figure 2 shows the integrated area under the XMCD curves, normalized to the low-temperature saturation value, as a function of temperature for the different applied pressures. The data show that the Curie temperature of $\text{Gd}_5(\text{Si}_{0.125}\text{Ge}_{0.875})_4$ is enhanced with pressure, from 80 K at ambient pressure to 257 K at $P=14.55$ GPa. This is the highest Curie temperature reported so far for this Ge-rich composition. (The Curie temperature is determined here from the maximum absolute value of the derivative of the fitted lines in Fig. 2.) Another notable feature of the data is the presence of a nonzero XMCD signal above T_c for $P=0.25, 1.36, 2.75, 3.86$ GPa, which is related to the AFM phase present in the low x region ($x \leq 0.2$) of the x - T phase diagram, as discussed below.

The ability to determine pressure *in situ* is demonstrated in Fig. 3, which shows the magnitude of the complex Fourier transform of Cu K -edge XAFS, data and fits, for $P=0$ and $P=14.55$ GPa. The data and fits shown in the Fourier transforms use a k -range from 2 to 10 \AA^{-1} , where k is the photoelectron wave number. The fitting model assumes a uniform compressibility of all Cu-Cu bonds, and the real-space fits include contributions from the first two atomic shells only. In addition to a clear shift to shorter distance with increased pressure, an increase in XAFS amplitude is also evident. This is due to the decrease in bond-length's vibrational disorder upon volume reduction. The pressure is obtained from the fitted volume change $\Delta V/V_0=3\Delta a/a_0$ (Δa is the change in bond length) using the compressibility curve of Cu at 300 K. This method yields pressure values with an absolute accuracy of ~ 0.5 –1 GPa, determined by the accuracy of XAFS for absolute distance determination (~ 0.002 – 0.005\AA). Relative changes in pressure, however, can be determined with a much higher accuracy of ~ 0.1 GPa.

The pressure dependence of T_c for $\text{Gd}_5(\text{Si}_{0.125}\text{Ge}_{0.875})_4$ and $\text{Gd}_5(\text{Si}_{0.5}\text{Ge}_{0.5})_4$ is summarized in Figs. 4(a) and 4(b), respectively. The dependence of T_c on x (ambient pressure) is superimposed to highlight the correspondence between x and P . The overlaying x scale is determined by using known $T_c(x)$ values from the literature² for $x=0.125, 0.5$, and 1.0 at $P=0$. One can see that the general features of $T_c(x)$ are also present in $T_c(P)$: namely a linear dependence of T_c on P , with a change in slope at $x \sim 0.5$. As we discuss below, an

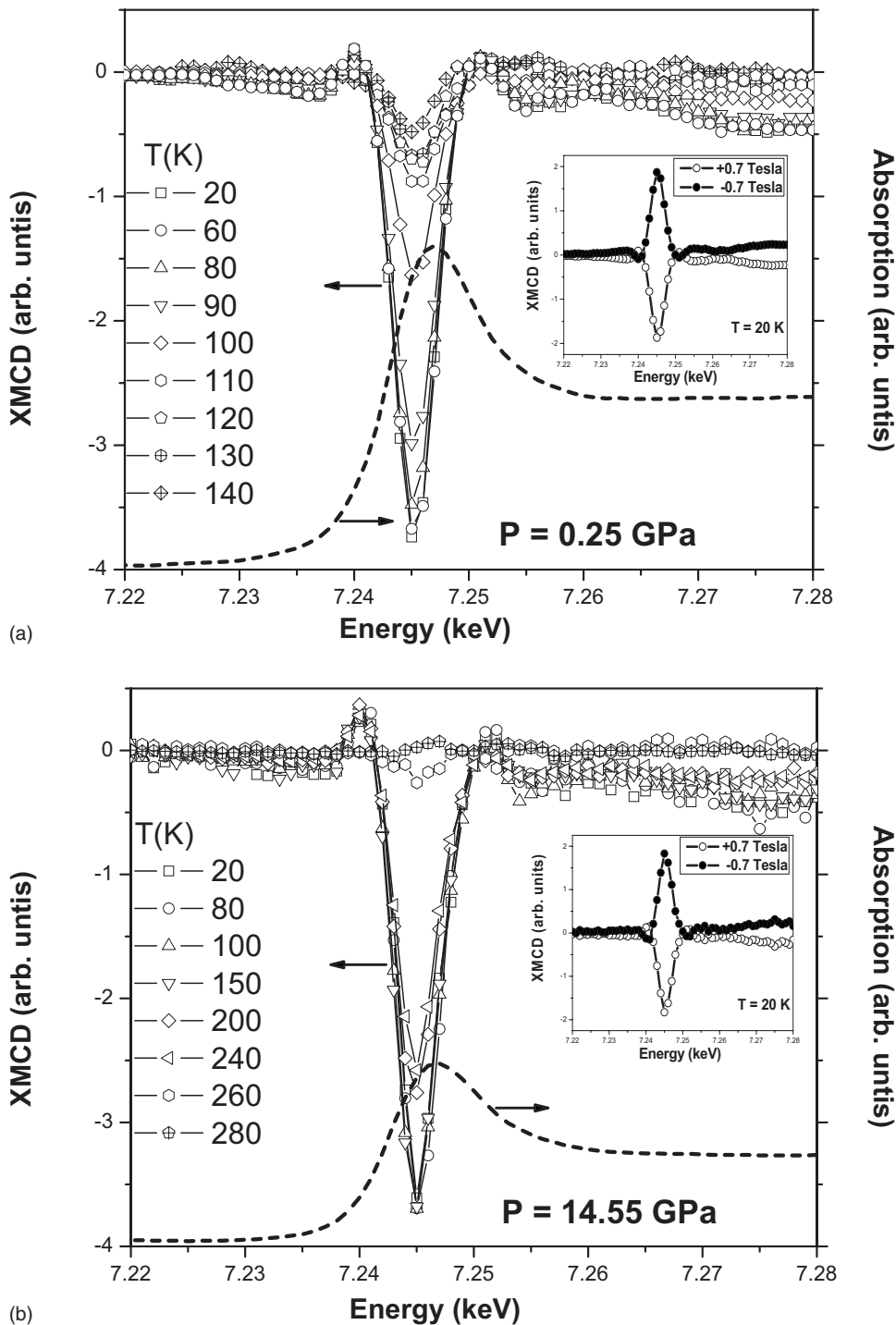


FIG. 1. Gd L_3 -edge XMCD signal (normalized to the absorption edge jump) as a function of temperature for (a) $P=0.25$ GPa and (b) $P=14.55$ GPa. The insets show the reversal of XMCD signal upon reversal of applied magnetic field. The helicity-independent absorption spectra, obtained as the average of absorption spectra for opposite helicities, is shown by the dashed lines. The sample thickness decreases with pressure causing a reduction in absorption edge jump. The absolute value of XMCD at low-temperature and $H=0.7$ Tesla is 1.4%, a reduction of $\sim \times 4$ relative to its saturation value at $H = 4$ T.

additional common feature is the disappearance of the FM-AFM transition on warming for $P > 4$ GPa. This transition manifests itself in the XMCD data as a nonzero signal above T_c .

IV. DISCUSSION

The nonzero XMCD signal above T_c for $P < 4$ GPa in Fig. 2 indicates the presence of a small ferromagnetic component. Nonzero magnetization above T_c with a similar ratio of $M_s/M_{\text{tail}} \sim 5.5$ was also observed in the SQUID data of

Morellon *et al.*⁴ for a $x=0.1$ compound. The low- x , Ge-rich compounds are known to undergo a FM-AFM transition at ambient pressure before they become paramagnetic at higher temperature. This intermediate transition is only observed for $x \leq 0.2$, while higher x samples directly transform into a paramagnetic phase on warming.^{2,6,7} The nonzero XMCD tail for $T > T_c$ is likely due to canting of the AFM structure induced by the applied field. For example, Gd_5Ge_4 , which is AFM at zero field displays significant canting in an applied field.¹⁵ The nonzero XMCD tail is not present in the $P = 14.55$ GPa data, indicating a direct transition from FM to

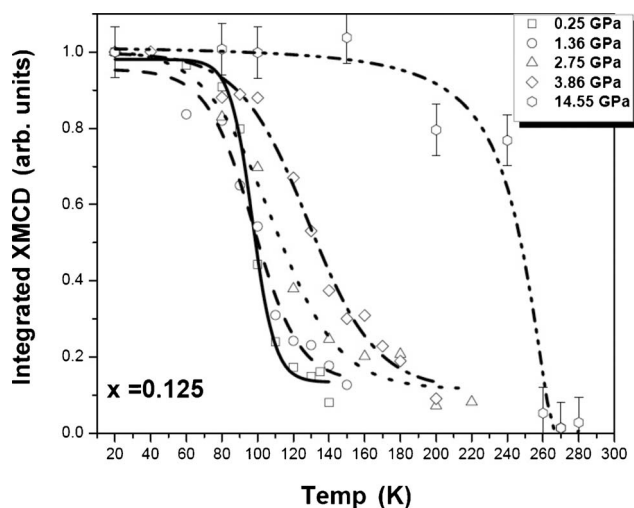


FIG. 2. Integrated XMCD as a function of temperature for different applied pressures. The XMCD signal is normalized to the saturation value at 20 K. The lines are guides to the eye. Error bars, shown for the $P=14.55$ GPa data, are the same for all data sets.

PM state at this pressure. The presence of a tail for $P < 4$ GPa [which in Fig. 4(a) is shown to be equivalent to $x \leq 0.22$] and its absence at $P=14.55$ GPa (equivalent to $x \sim 0.43$) is in agreement with the occurrence of the FM-AFM transition only at low x (low pressure) and its absence at high x (high pressure).

The $P(x)$ - T magnetic phase diagram shown in Fig. 4 highlights the relationship between pressure and Si doping. Starting with a $\text{Gd}_5(\text{Si}_{0.125}\text{Ge}_{0.875})_4$ sample, pressures of $P=0.25$, 1.36, 2.75, 3.86, and 14.55 GPa produce a temperature dependence of the magnetic structure corresponding to $x=0.14$, 0.15, 0.17, 0.22, and 0.44, respectively, resulting in $\Delta(\text{Si}\%)/\Delta P=0.205$ (Si%) kbar^{-1} [Fig. 4(a)]. The pressure dependence of the magnetic transition temperature is linear with a slope $dT_c/dP=1.2$ K kbar^{-1} . For comparison, a value

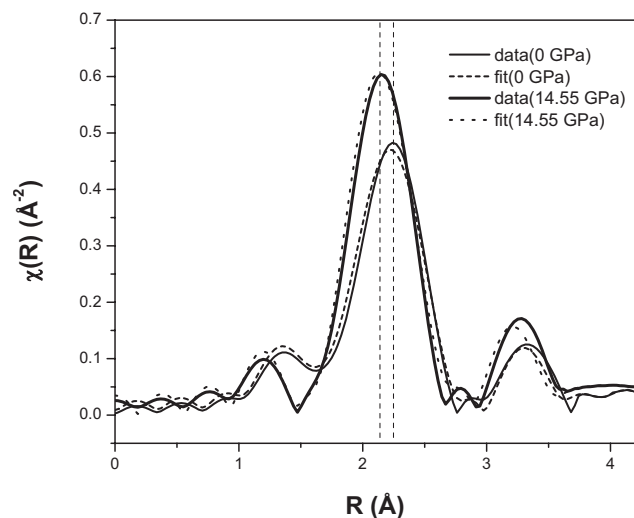


FIG. 3. Magnitude of the Fourier transform of $k\chi(k)$ for the Cu K edge at 300 K under $P=0$ and 14.55 GPa, respectively. The vertical dashed lines highlight the shift to lower interatomic distances with increased pressure.

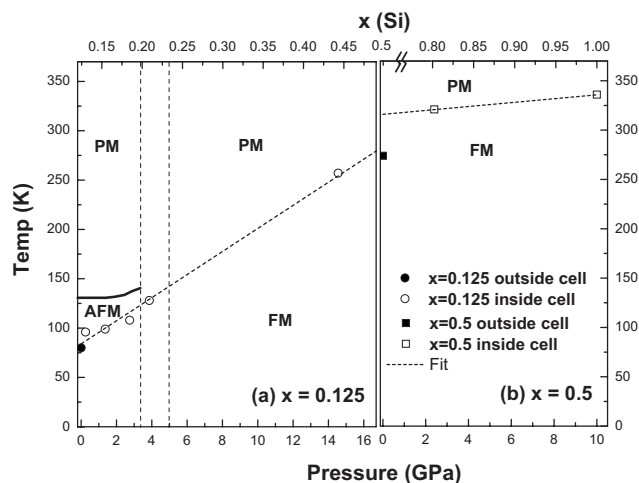


FIG. 4. Magnetic phase diagram as a function of Si concentration (top) and applied pressure (bottom). The points indicate the observed Curie temperatures, T_c , for different pressures as measured by XMCD for $x=0.125$ (a) and $x=0.5$ (b) samples. The “outside cell” data correspond to ambient pressure conditions.

of $dT_c/dP=3.0$ K kbar^{-1} was obtained in Ref. 13 for a limited pressure range below about 1.0 GPa.

The XMCD data measured on the $\text{Gd}_5(\text{Si}_{0.125}\text{Ge}_{0.875})_4$ sample outside the DAC at ambient pressure²⁷ show a Curie temperature of 80 K, which is in agreement with previous SQUID measurements^{2,6,7} and also very close to $T_c=84$ K found by a linear extrapolation to $P=0$ of the data in Fig. 4(a). At the other end of the x scale in this panel, a T_c of 284 K is found by extrapolating the fit to $x=0.5$, which is only 10 K higher than $T_c=274$ K directly measured in $\text{Gd}_5(\text{Si}_{0.5}\text{Ge}_{0.5})_4$ at ambient pressure²⁷ [shown by the filled square in Fig. 4(b)].

The data shown in Fig. 4(b) correspond to measurements performed on a $x=0.5$ sample. Applied pressures of $P=2.4$ and 10 GPa result in $T_c \sim 321$ and ~ 336 K, corresponding to the x values of 0.8 and 1.0, respectively.^{2,6,7} Interestingly, $\text{Gd}_5(\text{Si}_{0.5}\text{Ge}_{0.5})_4$ at an applied pressure of 10 GPa shows the same magnetic ordering temperature as pure Gd_5Si_4 with $T_c=336$ K. In addition, even though a $T_c \sim 336$ K is the ultimate transition temperature achieved by Si doping in the $\text{Gd}_5(\text{Si}_x\text{Ge}_{1-x})_4$ compounds, the data indicate that further increases in transition temperature are expected for pressures beyond 10 GPa. This means that hydrostatic pressure provides an additional, valuable route to T_c manipulation (albeit in a reversible way), because it is not limited by the end boundaries of the solid solution.

At ambient pressure, $\text{Gd}_5(\text{Si}_{0.5}\text{Ge}_{0.5})_4$ is located near a structural boundary. While it is monoclinic (M) at room temperature, a slight increase in Si concentration drives it into the orthorhombic [$O(I)$] phase with a concomitant increase in T_c . Since the compressibility of monoclinic and orthorhombic phases are markedly different,¹⁶ this structural transition is responsible for the observed discontinuity in dT_c/dx at $x \leq 0.5$.^{2,6,7} Similarly, pressure causes a first-order $M \rightarrow O(I)$ transition in $\text{Gd}_5(\text{Si}_{0.5}\text{Ge}_{0.5})_4$ within a pressure range $P \sim 1.0$ – 2.0 GPa,¹⁴ with T_c changing from 270 to 305 K. Our smallest pressure of $P=2.5$ GPa is enough to cause the

transition into the $O(I)$ phase, and this transition with its related T_c increase is responsible for the discontinuity in dT_c/dP . The slope of a fit through $P=2.4, 10$ GPa data points yields a $dT_c/dP=0.2$ K kbar $^{-1}$, similar to the 0.3 K kbar $^{-1}$ reported for a $x=0.8$ sample in Ref. 13 but lower than the 0.9 K kbar $^{-1}$ reported in Ref. 28. The correspondence between doping and pressure using the $x=0.5$ data in Fig. 4(b) is $\Delta(\text{Si}\%)/\Delta P=0.26$ (Si%) kbar $^{-1}$, which is comparable to 0.205 (Si%) kbar $^{-1}$ obtained using the $x=0.125$ data in Fig. 4(a).

The results clearly demonstrate that the FM \rightarrow PM transition in $\text{Gd}_5(\text{Si}_x\text{Ge}_{1-x})_4$ alloys can be similarly affected by Si doping and applied pressure, at least in a qualitative way. Magnetic interactions between localized Gd $4f$ moments are indirect since there is virtually no overlap between Gd $4f$ wave functions. Most intermetallic alloys exhibit an indirect Ruderman-Kittel-Kasuya-Yosida (RKKY) coupling²⁹ through a spin-polarized conduction band. While this is likely the dominant mechanism for exchange coupling between Gd ions inside Gd slabs (intraslab), it has also been argued⁶ that an indirect superexchange coupling³⁰ plays a role in mediating interslab coupling through the intervening, nonmagnetic Ge(Si)-Ge(Si) bonds that connect the Gd slabs in the FM, orthorhombic structure. The recent observation of magnetic polarization in Ge $4p$ orbitals due to hybridization with Gd $5d$ orbitals, however, indicates that RKKY coupling may also be involved in mediating interlayer magnetic coupling.²⁷ Regardless of whether the indirect, interslab coupling is of the RKKY or superexchange type, its strength is intimately connected with the overlap of Gd $5d$ and Ge $4p$ (Si $3p$) states. This overlap is enhanced by a volume contraction induced by either Si doping or applied pressure. For superexchange interactions, the increased overlap of magnetic Gd $5d$ and nonmagnetic Ge $4p$ (Si $3p$) states increases the probability for virtual hopping needed to mediate Gd-Gd indirect exchange. For RKKY interactions, the increased overlap between Gd $5d$ and Ge $4p$ (Si $3p$) states promotes hybridization and the related ability to transfer magnetic interactions through a spin-polarized Gd $5d$ -Ge $4p$ (Si $3p$) conduction band.

Pressure studies allow to unambiguously distinguish between volume-driven and other possible doping-induced effects upon the magnetic properties of these materials. In addition to volume-driven effects, doping may result in (a) nonrandom distribution of Si/Ge among the three inequivalent crystal sites,³¹ (b) volume-independent modifications to the electronic structure due to differences in Ge $4p$ and Si $3p$ wave functions, and (c) phase separation or spatially inhomogeneous distribution of Si dopants in the host matrix depending on the conditions of the material's synthesis. Our observation that the application of pressure in an extended range is able to reproduce all of the features in the x - T magnetic phase diagram may be interpreted as an indication that, at least qualitatively, volume-driven effects can account for the observed Si-induced changes in the x - T magnetic phase diagram. However, evaluating the quantity $\gamma_M = -(\Delta T_c/T_c)/(\Delta V/V)$, where $\Delta V/V$ is the fractional change in volume induced by pressure or doping, provides a measure of the efficiency by which a structural volume change is

converted into a change in T_c . Such comparison requires knowledge of the material's compressibility, which we have not measured. Using the compressibility value of $\kappa=-0.25$ Mbar $^{-1}$ in Ref. 14, and the doping-dependent lattice parameters in Ref. 32, we estimate that Si doping is ~ 3 times more effective in increasing T_c than pressure is for a given volume change. In other words, obtaining a similar increase in T_c requires a threefold larger volume reduction with pressure than it does with doping. This is in agreement with the conclusions in Ref. 13, and indicates that Si doping does more to stabilize ferromagnetic interactions than simply *uniformly* reducing the volume of the unit cell. Electronic structure calculations³¹ show very small changes in the spin-polarized Gd $5d$ band upon substitution of Si for Ge. However, these calculations cannot account, and therefore neglect the *local*, nonperiodic volume contraction that is expected to occur as a result of the smaller atomic size of Si. This local fractional volume change $(\Delta V/V)_{\text{local}}$ is expected to be significantly larger than the macroscopic volume change measured by diffraction techniques (larger by $\sim x^{-1}$ in the diluted-Si limit). Pressure, on the other hand, compresses the lattice uniformly. One may speculate that the largely compressed local regions around Si dopants act more efficiently as local FM exchange pathways, much like filaments in a network, stabilizing FM order faster than a smaller, uniform compression of the lattice.

V. SUMMARY

Using XMCD we have demonstrated that applying hydrostatic pressure yields similar, qualitative magnetic behavior to that obtained by Si doping in $\text{Gd}_5(\text{Si}_x\text{Ge}_{1-x})_4$ ($x=0.125, 0.5$) over a large pressure range up to ~ 15 GPa. This correspondence is quantified to be $\Delta(\text{Si}\%)/\Delta P=0.233$ (Si%) kbar $^{-1}$. A number of features in the x - T magnetic phase diagram of these materials are also obtained here by applying pressure, namely, the disappearance of the intermediate AFM phase, a linear increase in T_c and a discontinuity in dT_c/dP at $T_c \sim 275$ K. Based on the reported compressibility and doping-dependent lattice parameters for these compounds, our results indicate that Si doping does more to stabilize FM interactions in these materials than is achieved by an equivalent, *uniform* reduction in lattice volume alone. We speculate that the local compression of the lattice around Si atoms, which is expected to be larger than the averaged volume reduction measured by crystallography, may be an important parameter in fully understanding the correspondence between Si doping and applied pressure. Further theoretical and experimental efforts are needed to address this point, with local structural probes³³ expected to play a predominant role.

ACKNOWLEDGMENTS

The work at Argonne and Ames is supported by the U.S. Department of Energy, Office of Science, under Contracts Nos. DE-AC-02-06CH11357 and DE-AC02-07CH11358, respectively. The authors would like to thank Y. Ding and Y. Feng for help with the pressure cell.

*haskel@aps.anl.gov

- ¹V. K. Pecharsky, and K. A. Gschneidner, Jr., *Phys. Rev. Lett.* **78**, 4494 (1997).
- ²V. K. Pecharsky and K. A. Gschneidner, Jr., *Appl. Phys. Lett.* **70**, 3299 (1997).
- ³Z. B. Guo, J. R. Zhang, H. Huang, W. P. Ding, and Y. W. Du, *Appl. Phys. Lett.* **70**, 904 (1997).
- ⁴L. Morellon, J. Blasco, P. A. Algarabel, and M. R. Ibarra, *Phys. Rev. B* **62**, 1022 (2000).
- ⁵V. K. Pecharsky and K. A. Gschneidner, Jr., *J. Magn. Magn. Mater.* **200**, 44 (2001).
- ⁶V. K. Pecharsky and K. A. Gschneidner, Jr., *Adv. Mater. (Weinheim, Ger.)* **13**, 683 (2000).
- ⁷V. K. Pecharsky and K. A. Gschneidner, Jr., *J. Alloys Compd.* **260**, 98 (1997).
- ⁸A. O. Pecharsky, K. A. Gschneidner, Jr., and V. K. Pecharsky, *J. Appl. Phys.* **93**, 4722 (2003).
- ⁹W. Choe, V. K. Pecharsky, A. O. Pecharsky, K. A. Gschneidner, Jr., V. G. Young, Jr., and G. J. Miller, *Phys. Rev. Lett.* **84**, 4617 (2000).
- ¹⁰A. Giguere, M. Foldeaki, B. Ravi Gopal, R. Chahine, T. K. Bose, A. Frydman, and J. A. Barclay, *Phys. Rev. Lett.* **83**, 2262 (1999).
- ¹¹K. A. Gschneidner, Jr., V. K. Pecharsky, E. Bruck, H. G. M. Duijn, and E. M. Levin, *Phys. Rev. Lett.* **85**, 4190 (2000).
- ¹²V. K. Pecharsky, A. P. Holm, K. A. Gschneidner, Jr., and R. Rink, *Phys. Rev. Lett.* **91**, 197204 (2003).
- ¹³L. Morellon, Z. Arnold, P. A. Algarabel, C. Magen, M. R. Ibarra, and Y. Skorokhod, *J. Phys.: Condens. Matter* **16**, 1623 (2004).
- ¹⁴Ya. Mudryk, Y. Lee, T. Vogt, K. A. Gschneidner, Jr., and V. K. Pecharsky, *Phys. Rev. B* **71**, 174104 (2005).
- ¹⁵L. Tan, A. Kreyssig, J. W. Kim, A. I. Goldman, R. J. McQueeney, D. Wermeille, B. Sieve, T. A. Lograsso, D. L. Schlagel, S. L. Budko, V. K. Pecharsky, and K. A. Gschneidner, Jr., *Phys. Rev. B* **71**, 214408 (2005).
- ¹⁶C. Magen, L. Morellon, P. A. Algarabel, M. R. Ibarra, Z. Arnold, J. Kamarad, T. A. Lograsso, D. L. Schlagel, V. K. Pecharsky, A. O. Tsokal, and K. A. Gschneidner, *Phys. Rev. B* **72**, 024416 (2005).
- ¹⁷G. Schutz, W. Wagner, W. Wilhelm, P. Kienle, R. Zeller, R. Frahm, and G. Materlik, *Phys. Rev. Lett.* **58**, 737 (1987); P. Carra and M. Altarelli, *ibid.* **64**, 1286 (1990); J. Stohr, *J. Magn. Magn. Mater.* **200**, 470 (1997).
- ¹⁸E. A. Stern, *Philips Tech. Rev.* **10**, 3027 (1974); P. A. Lee and J. B. Pendry, *Phys. Rev. B* **11**, 2795 (1975).
- ¹⁹A. Dadashev, M. P. Pasternak, G. Kh. Rozenberg, and R. D. Taylor, *Rev. Sci. Instrum.* **72**, 2633 (2001).
- ²⁰J. W. Freeland, J. C. Lang, G. Srajer, R. Winarski, D. Shu, and D. M. Mills, *Rev. Sci. Instrum.* **73**, 1408 (2002).
- ²¹K. Hirano, K. Izumi, T. Ishikawa, S. Annaka, and S. Kikuta, *J. Appl. Phys.* **30**, L407 (1991).
- ²²J. C. Lang and G. Srajer, *Rev. Sci. Instrum.* **66**, 1540 (1995).
- ²³M. Suzuki, N. Kawamura, M. Mizumaki, A. Urata, H. Maruyama, S. Goto, and T. Ishikawa, *Jpn. J. Appl. Phys., Part 2* **37**, L1488 (1998).
- ²⁴S. I. Zabinsky, J. J. Rehr, A. Ankudinov, R. C. Albers, and M. J. Eller, *Phys. Rev. B* **52**, 2995 (1995).
- ²⁵<http://cars9.uchicago.edu/ifeffit/>
- ²⁶A. Dewaele, P. Loubeyre, and M. Mezouar, *Phys. Rev. B* **70**, 094112 (2004).
- ²⁷D. Haskel, Y. B. Lee, B. N. Harmon, Z. Islam, J. C. Lang, G. Srajer, Ya. Mudryk, K. A. Gschneidner, Jr., and V. K. Pecharsky, *Phys. Rev. Lett.* **98**, 247205 (2007).
- ²⁸A. Magnus, G. Carvalho, C. S. Alves, A. de Campos, A. A. Coelho, S. Gama, F. C. G. Gandra, P. J. von Ranke, and N. A. Oliveira, *J. Appl. Phys.* **97**, 10M320 (2005).
- ²⁹M. A. Ruderman and C. Kittel, *Phys. Rev.* **96**, 99 (1954); T. Kasuya, *Prog. Theor. Phys.* **16**, 45 (1956); K. Yosida, *Phys. Rev.* **106**, 893 (1957).
- ³⁰P. W. Anderson, *Phys. Rev.* **79**, 350 (1950).
- ³¹D. Paudyal, V. K. Pecharsky, K. A. Gschneidner, Jr., and B. N. Harmon, *Phys. Rev. B* **73**, 144406 (2006).
- ³²A. O. Pecharsky, K. A. Gschneidner, Jr., V. K. Pecharsky, and C. E. Schindler, *J. Alloys Compd.* **126**, 338 (2002).
- ³³D. Haskel, E. A. Stern, F. Dogan, and A. R. Moodenbaugh, *Phys. Rev. B* **61**, 7055 (2000); D. Haskel, E. A. Stern, V. Polinger, and F. Dogan, *ibid.* **64**, 104510 (2001); E. Kravtsov, D. Haskel, A. Cady, A. Yang, C. Vittoria, X. Zuo, and V. G. Harris, *ibid.* **74**, 104114 (2006).